Robust Track-Following for Dual-Stage Servo Systems by Sensitivity Shaping with Degree Constraint

Ryozo Nagamune, Xinghui Huang, and Roberto Horowitz

Department of Mechanical Engineering

University of California, Berkeley, CA 94720-1740

{ryozo,xhhuang,horowitz}@me.berkeley.edu

Abstract

This paper presents track-following control design, with a new sensitivity shaping technique, for dual-stage servo systems in hard disk drives. The shaping technique simultaneously takes care of both complexity of controllers and robustness, important issues for controller implementation. As dual-stage servo systems, in addition to the conventional voice coil motor, a microactuator at the slider is adopted. Using these actuators, two types of feedback structures are to be considered; one is the structure for the sensitivity decoupling method, and the other is for the PQ method. After controller design, robust stability and robust performance against parametric uncertainties are evaluated. The simulation results show that, with the new shaping technique, nominal performance of track-following can be improved without losing robust stability.

Key Words: Dual-stage servo system, sensitivity shaping, controller complexity, robustness.

1 Introduction

Track-following control of the magnetic head is of great importance in increasing the track density in hard disk drives (HDDs) [1]. Traditionally, for the servo control in HDDs, the voice coil motor (VCM) and the position error signal (PES) have been used as an actuator and a feedback signal of the control system. However, this structure has severe limitations on achievable tracking performance, especially caused by the low sampling-rate of the PES [16] and mechanical resonance modes of the actuator [4]. To push forward the limitations and to improve the tracking performance, *dual-stage servo systems*, which utilizes a secondary actuator, have been developed and intensively investigated; see e.g. [1, 6, 14]. Multi-sensing has also been exploited for further performance improvement [4, 6].

With auxiliary information available, controller design for dual-stage servo systems is essentially a multivariable control problem, and there are roughly two kinds of approaches to such design, i.e., an approach based on classical SISO control techniques such as PID and lead-lag controllers [11, 5, 13], and an approach based on modern robust control theories such as H^∞ and μ controllers [2, 6]. The former approach confines feedback structures so that the whole design can be divided into a series of scalar control problems, while the latter approach directly solves the multivariable problem. In this paper, we take the former approach, but with a method different from classical methods.

Mathematically, the performance of track-following in HDDs is evaluated in terms of the RMS value of the PES against all the modeled exogenous signals (track runout, measurement noises, windage, etc.). The RMS value has to be small for good track-following. For *robust* track-following, that value should be small even with the plant perturbation. In addition, this must be achieved without violating the stability. Such robustness issues are critical to practical implementation since the plant dynamics varies from disk to disk during batch fabrication. Including all

these requirements at once makes the controller design quite complicated and hard to solve. To make matters worse, the controller order is likely to become too high to implement in HDDs.

In this paper, we propose an alternative design approach to solve the robust track-following problem in HDDs. The design consists of two stages. In the first stage, we design a "preliminary" controller by the conventional lead-lag compensations. In the second stage, we modify the closed-loop performance given by this controller. There are several modifications that can be considered. For example, we can improve the nominal performance at the expense of less robust stability margin. On the other hand, we can also enhance robust performance by sacrificing nominal performance. For these modifications, we try to change the shape of the sensitivity frequency response. This is reasonable since the sensitivity function captures, to a large extent, essential properties of the closed-loop system, such as tracking, noise rejection and robust stability. For the design in the second stage, we will employ the shaping technique of the sensitivity frequency response, recently developed in [7]. The controller order designed in the second stage is bounded by a certain order similar to that of the plant used for the design.

This paper is organized as follows. In Section 2, a dual-stage servo system considered in this paper is briefly explained. The system is the same as the one treated in [3]. A robust track-following problem is also formulated in Section 2. To solve this control problem, a novel technique to sensitivity shaping is utilized, and it is reviewed in Section 3. Using the shaping technique, in Section 4, track-following controllers are synthesized for the dual-stage servo system, that is the main contribution of this paper. Two types of feedback structures are considered, that is, the structures for the sensitivity decoupling method and for the PQ method. For the designed controllers, nominal performance is computed, and robust stability and robust performance are analyzed with respect to parametric uncertainties.

2 Dual-stage servo system

In this section, we will briefly explain the dual-stage servo system considered in this paper. See [3] for complete descriptions of the system and the mathematical model. The dual-stage servo system has two actuators, i.e., a voice coil motor and a secondary microactuator fabricated using MEMS techniques (MEMS microactuator). After describing the dual-stage servo system, we will pose the robust track-following control problem to be considered in this paper.

2.1 Voice coil motor

The first actuator to be used for track-following is a conventional one, i.e., the voice coil motor (VCM). A mathematical model for the VCM, whose input is the current in VCM and the output is the generated head motion, can be modeled as a sum of seven resonance modes:

$$G_v(s) := \sum_{k=0}^{6} K_{vk} \frac{\omega_k^2}{s^2 + 2\zeta_k \omega_k + \omega_k^2}, \tag{1}$$

where the nominal values of the parameters $\{(K_{vk}, \zeta_k, \omega_k)\}_{k=0}^{6}$ are shown in Table 1. The Bode plot of G_v is depicted in Figure 1.

mode	0	1	2	3	4	5	6
$\omega_k/2\pi$ (Hz)	60	5275	7400	9144	10698	13002	15197
ζ_k	0.5	0.015	0.015	0.015	0.015	0.015	0.015
K_{vk}	14000	-0.0024	-0.0102	-0.8400	-0.3000	-0.0360	0.0102

Table 1: Nominal values of parameters in the VCM model G_v.

There exist some resonance modes in G_v in the high frequency range. Further increase of the servo bandwidth is thus limited by the presence of these modes. Furthermore, they may be excited by airflow turbulence and are difficult to suppress

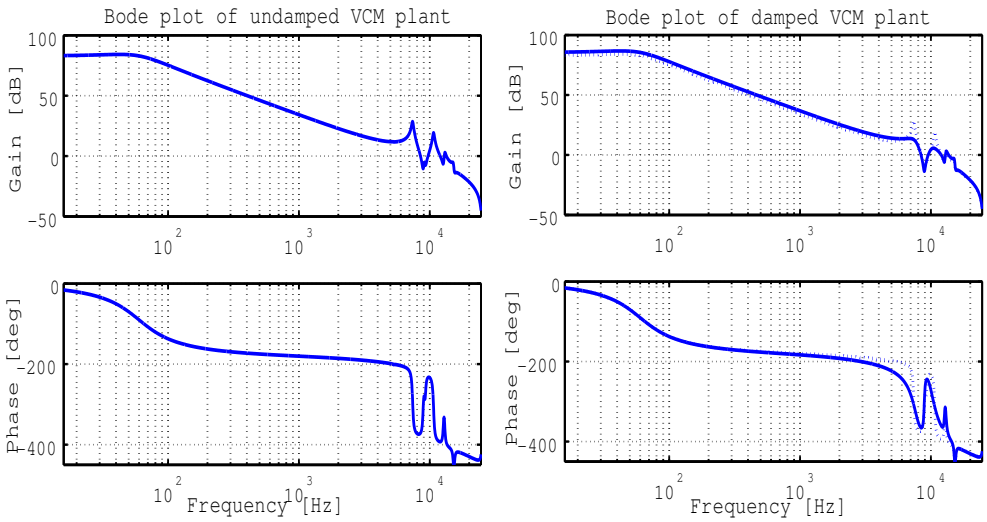

Figure 1: Bode plots of G_v (left) and $\hat{G}_v$ (right).

due to the limited sampling rate of the PES. To solve this problem, an instrumented suspension with PZT sensors attached on it is used. Using the signal from PZT sensors, we design an inner-loop damping controller by means of the LQG technique; see the control structure in Figure 2. The sampling frequency is assumed to be 50kHz. The damped VCM plant is of order 18. We can reduce the order to 14 without any significant change of the frequency response. We will denote this reduced-order plant by $\hat{G}_v$, and its input and output by u_v and y_v, respectively. In Section 4, for the controller design, we shall use this reduced model $\hat{G}_v$, while the robustness analysis after the design will be done with the original (not reduced) model, taking into account parametric uncertainties in ζ_k and ω_k. The Bode plot of $\hat{G}_v$ is shown in Figure 1.

2.2 Microactuator

As a secondary actuator, we will utilize a microactuator (MA) fabricated using MEMS techniques, which is placed between the suspension tip and the slider and actuates the slider relative to the suspension. Regarding the voltage to MA as an

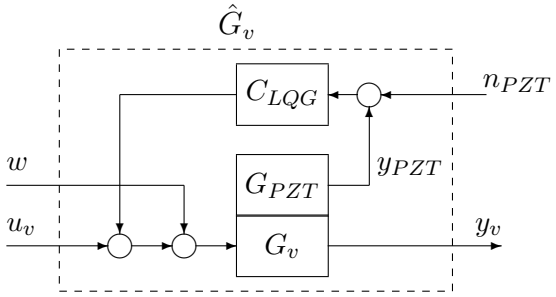

Figure 2: The structure of inner-loop damping control for VCM. G_{PZT} is the transfer function from the current u_v to the PZT sensor output, and w is the airflow turbulence.

input and the generated head motion as an output, a mathematical model of MA can be expressed as

$$G_m(s) := K_m \frac{\omega_m^2}{s^2 + 2\zeta_m\omega_m + \omega_m^2}, \tag{2}$$

where the nominal values of (K_m, ζ_m, ω_m) are shown in Table 2. The Bode plot of G_m is shown in Figure 4.

mode	MA
$\omega_m/2\pi$ (Hz)	2250
ζ_m	0.2
K_m	0.2

Table 2: Nominal values of parameters in the MA model G_m.

The resonance mode of MA is also undesirable for achieving high performance. A damping controller is designed using pole-placement [3], and closed around the MA, as shown in Figure 3. We denote the damped MA by $\hat{G}_m$, whose Bode plot is depicted in Figure 4. Again, the sampling frequency is set to 50kHz in the damping design.

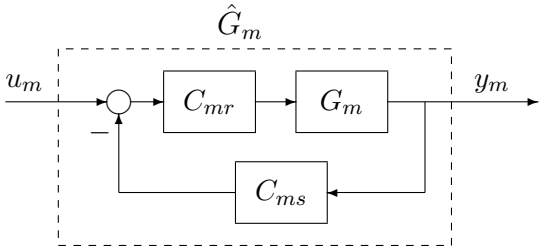

Figure 3: The structure of inner-loop damping control for MA. The controllers for pole-placement are C_{mr} and C_{ms}.

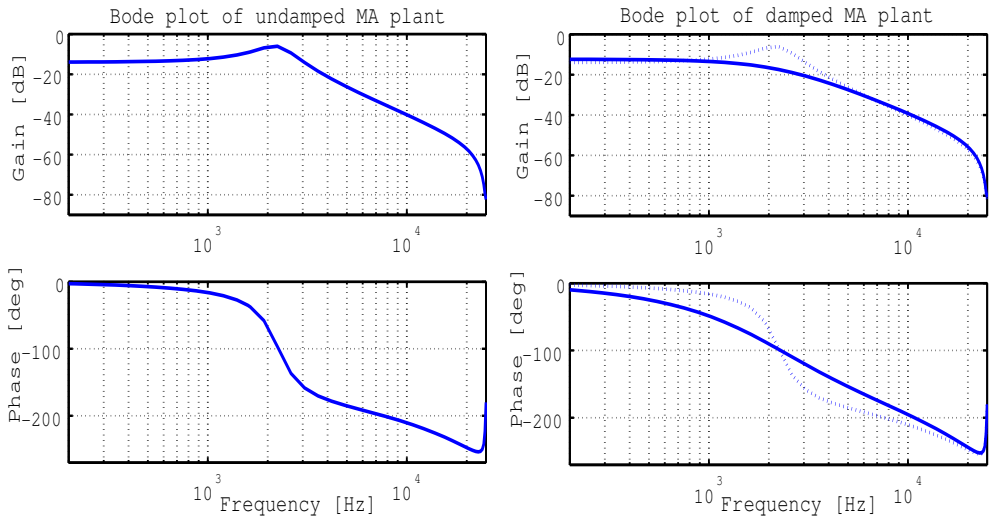

Figure 4: Bode plots of G_m (left) and $\hat{G}_m$ (right).

2.3 Interconnection of VCM and MA

Using the damped VCM plant $\hat{G}_v$ and the damped MA plant $\hat{G}_m$, we now interconnect these plants to construct a dual-stage servo system for track-following control. The interconnection depends on the type of MA, that is, on whether the MA is rotational [15] or translational [8].

If we consider a rotational MA, the transfer function from u_v to y_h (head position) is simply $\hat{G}_v$, and is independent of MA; see the left figure in Figure 5. On the other hand, if we consider a translational MA, the transfer function from u_v to y_h *does* depend on some parameters in the MA. This dependence is shown in the right figure

of Figure 5, where

$$G_{mTr} := \frac{s^2}{s^2 + 2\xi_m \omega_m s + \omega_m^2}. \tag{3}$$

Notice that taking $G_{mTr} = 0$ in Figure 5 reduces the structure of the dual-stage servo system with a translational MA to the one with a rotational MA. In the case with a translational MA, we can simply write

$$y_h = \tilde{G}_v u_v + \hat{G}_m u_m, \tag{4}$$

with an appropriate transfer function $\tilde{G}_v$. We denote systems surrounded by dashed lines in Figure 5 by G_R and G_T, where "R" and "T" stand for "Rotational" and "Translational," respectively.

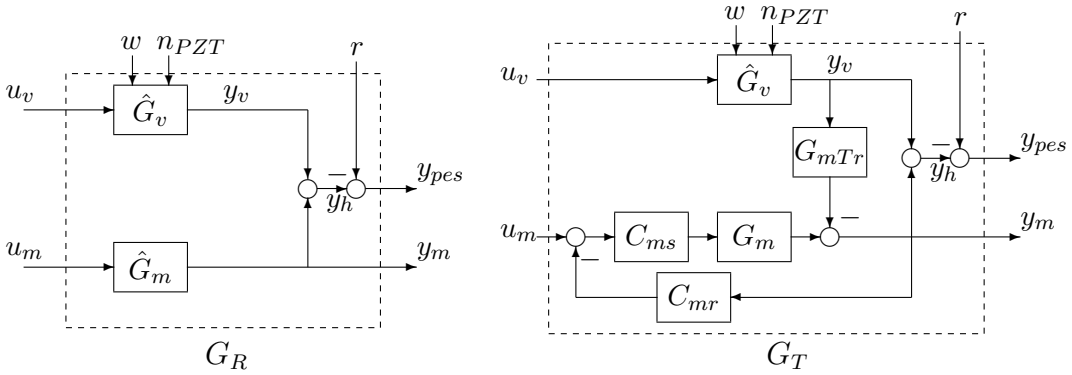

Figure 5: Dual-stage servo systems for track-following control in the case of a rotational MA (left figure) and a translational MA (right figure).

In Figure 5, the PES is denoted by y_{pes}, and the runout, denoted by r, is a signal after a white noise has passed through a shaping filter

$$W_r(s) := \frac{200\omega_r^2}{s^2 + 1.6\omega_r + \omega_r^2} + \frac{5000}{s + 2\omega_r}, \quad \omega_r := 300\pi. \tag{5}$$

2.4 Robust track-following control problem

Now, using the dual-stage servo system constructed in the previous subsection, we shall pose the robust track-following control problem to be tackled in Section 4 as

follows.

Given the dual-stage servo system in Figure 5, design a controller whose inputs are y_{pes} and y_m and outputs are u_v and u_m, such that the closed-loop system maintains stability even with uncertainties in G_v and G_m, and has a small RMS value of y_{pes} against all the disturbances (windage, measurement noise and runout). The RMS value should not increase so much with perturbations of parameters in G_v and G_m. This should be achieved with controllers of low order for implementation.

This is a multivariable control problem. There are generally two approaches to the problem. One is to treat a multivariable problem as a series of scalar problems, and the other is to directly solve the multivariable problem. In this paper, we take the former approach in order to use a controller design technique recently developed for scalar problems. In the next section, we will briefly review the technique which will be used in Section 4. For complete expositions of the design technique, see [7].

3 Sensitivity shaping with degree constraint

Consider a feedback system in Figure 6. Here, G is a given scalar real rational transfer function in discrete-time and C is a scalar controller to be designed. The transfer function from r to y is called the *sensitivity function*, and given by

$$S := \frac{1}{1+GC}. \tag{6}$$

Notice that designing C and designing S are equivalent. In our approach, we focus on designing S, and after the design of S, we compute $C := (1-S)/GS$.

In this technique, it is assumed that a "desired" frequency response $\{s_k\}_{k=1}^N \subset \mathbb{C}$ is given at a finite number of frequencies $\{\theta_k\}_{k=1}^N \subset [0,\pi]$, and we try to find an S which fits well to the desired frequency response. This curve fitting problem can be depicted as in Figure 7. The distance between the desired frequency response and an S is measured by a squares sum. Mathematically, we need to solve a nonlinear

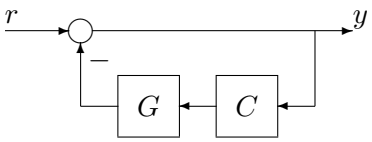

Figure 6: A feedback system.

least-squares optimization problem:

$$\min_{S\in\mathcal{S}} \sum_{k=1}^{N} w_k^2 \left| S(e^{i\theta_k}) - s_k \right|^2,$$

where the scalars w_k, $k = 1, \ldots, N$, are frequency weights to be adjusted by the designer. The domain $\mathcal{S}$ of the optimization problem is a set of sensitivity functions stabilizing the feedback system and satisfying a certain degree constraint. By this approach, we can search for appropriate controllers whose degrees are bounded by a degree similar to $\deg G$; see [7, Proposition 2.1]. Algorithms to solve the optimization problem have been provided in [7], and a user-friendly interface in MATLAB has been developed.

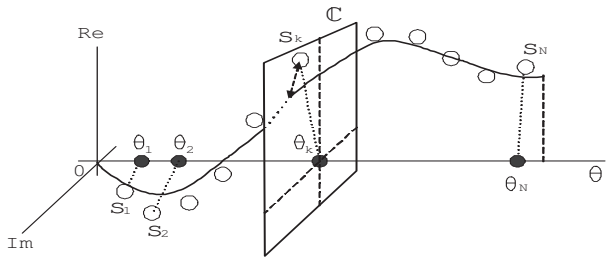

Figure 7: The frequency response of S (solid curve) and a desired frequency response $\{s_k\}_{k=1}^N$ (circles) at frequencies $\{\theta_k\}_{k=1}^N$ (black dots on θ-axis).

4 Controller designs by sensitivity shaping

In this section, we shall apply the sensitivity shaping technique in the previous section to robust track-following controller design for the dual-stage servo system

presented in Section 2. Two types of feedback structures are considered, that is, the structures for the sensitivity decoupling method and for the PQ method. In both design, we down-sample the model of the dual-stage servo system presented in Section 2 from 50kHz to 25kHz.

4.1 Sensitivity decoupling method

First, we will design track-following controllers using the feedback structure in Figure 8, where we consider a rotational MA. Control design using this structure is called the *sensitivity decoupling method*, since the sensitivity function S from the runout r to PES y_{pes} can be decoupled as a product of two sensitivity functions:

$$S = S_m S_v, \quad S_m := \frac{1}{1 + \hat{G}_m C_m}, \; S_v := \frac{1}{1 + \hat{G}_v C_v}. \tag{7}$$

See also Figure 9 illustrating the transfer function from runout to PES. This structure simplifies the design of controllers C_v and C_m, since a multivariable controller design problem can be transformed into two scalar problems, for which a number of simple design techniques are available. We shall apply the sensitivity shaping technique in Section 3 to the design of C_v and C_m.

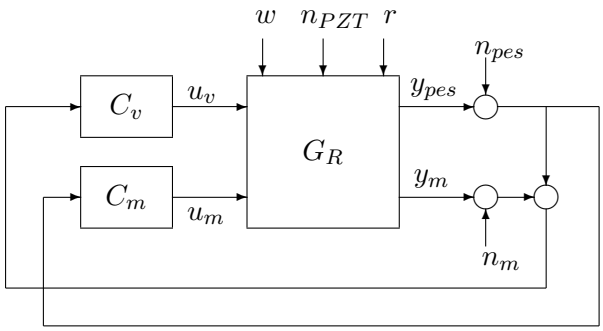

Figure 8: A structure for the sensitivity decoupling design.

To obtain a desired sensitivity function, as "initial" controllers, we use con-

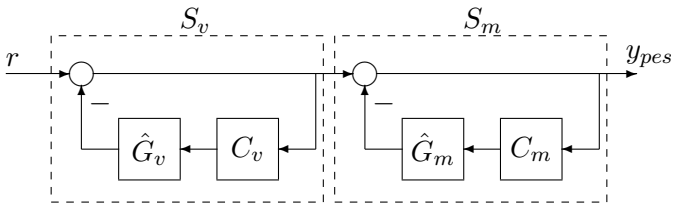

Figure 9: The transfer function from r to y_{pes}.

trollers, with sampling frequency 25kHz, designed via a classical control technique:

$$C_v^0 = \frac{0.01251z^2 - 0.02437z + 0.01186}{z^2 - 1.668z + 0.6687},\ C_m^0 = \frac{27.56z - 17.21}{z + 0.5715}. \tag{8}$$

The corresponding sensitivity functions are denoted by S_v^0 and S_m^0, respectively.

For the initial controllers above, the closed-loop performance has been examined. *Nominal performance*, which is the RMS (or σ-) value of PES against all exogenous signals (windage, noise and runout), is calculated as 6.6757. For *robust stability*, we assume real parametric uncertainties in G_v (see (1)) and G_m (see (2)) as in Table 3. Robust stability has been verified with μ-analysis [9]; see the μ-plot in Figure 10.

	parameter	uncertainty (%) of nominal values
G_v	$\omega_k,\ k = 1, \ldots, 6$	8
	$\zeta_k,\ k = 1, \ldots, 6$	20
G_m	ω_m	12
	ζ_m	25

Table 3: Parametric uncertainties in G_v and G_m.

Now, we modify the Bode plots of S_v^0 and S_m^0, in order to improve nominal performance without violating robust stability. To this end, we extract desired frequency responses $\{s_k\}_{k=1}^N$ for both S_v^0 and S_m^0, and modify them appropriately. The Bode plots for the designed S_v, S_m and S are drawn in Figure 11, and the performances are summarized in Table 4. Nominal performance and robust performance

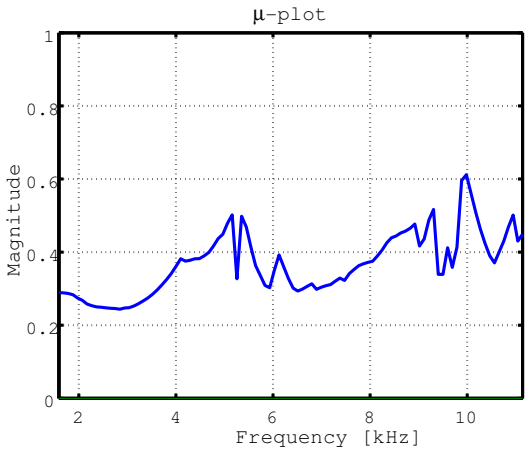

Figure 10: μ plot for parametric uncertainties (initial design).

have been improved by about 6% and 5.4%, respectively. Robust stability of the closed-loop system is also maintained as shown in Figure 12. The controller degrees are $\deg C_v = 15$ and $\deg C_m = 5$, which are much higher than the initial design, but they are considered to be acceptable for implementation by means of digital signal processors.

	NP	RP	BW (Hz)	LFG (dB)	$\deg C_v$	$\deg C_m$
initial design	6.6757	12.1916	2663.8	-84.25	2	1
final design	6.2740	11.5316	2344.2	-78.85	15	5

Table 4: Summary of performances: NP, RP, BW and LFG stand for nominal performance and robust performance of the feedback system, and bandwidth and low frequency gain of sensitivity functions, respectively.

4.2 PQ method

Next, for robust track-following controller design, we will combine the so-called PQ method proposed in [12] with the sensitivity shaping technique in Section 3. The

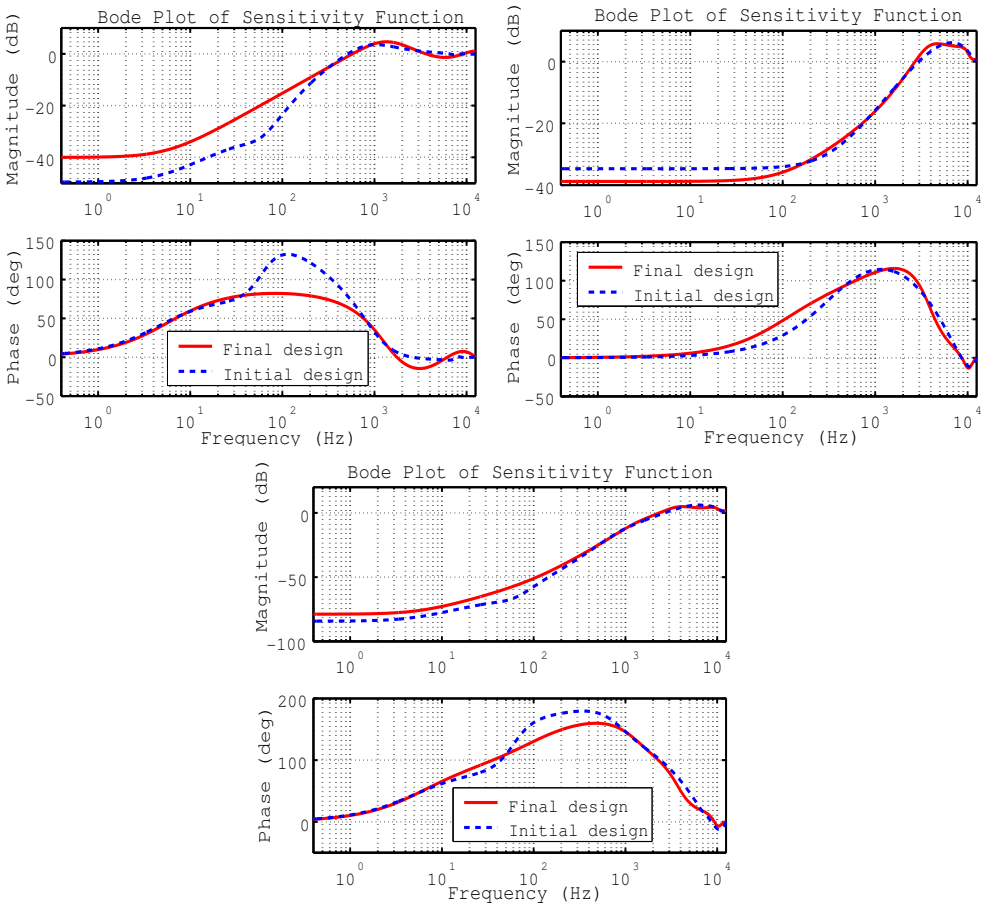

Figure 11: Bode plots of S_v (left-upper), S_m (right-upper) and $S = S_v S_m$ (lower).

control structure is depicted in Figure 14, where we consider a translational MA. In Figure 14, G_T is given in (5). The transfer function from r to y_{pes} is depicted in Figure 15, where $\tilde{G}_v$ and $\hat{G}_m$ are given in (4). The controllers P and Q have been designed by the PQ methods, avoiding the conflict of control between P and Q; see [12]. The system $G := \tilde{G}_v Q + \hat{G}_m P$, the part surrounded by the dashed line in Figure 15, has become of order 25. With model reduction, we have reduced the order of G to 15 without changing its frequency response so much.

Now, we design a controller C in Figure 14. The first attempt is a lead-lag

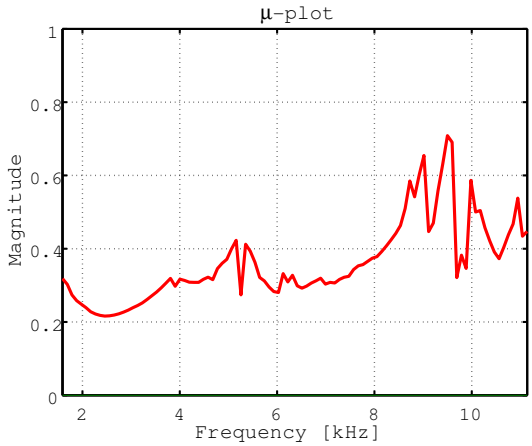

Figure 12: μ plot for parametric uncertainties (final design).

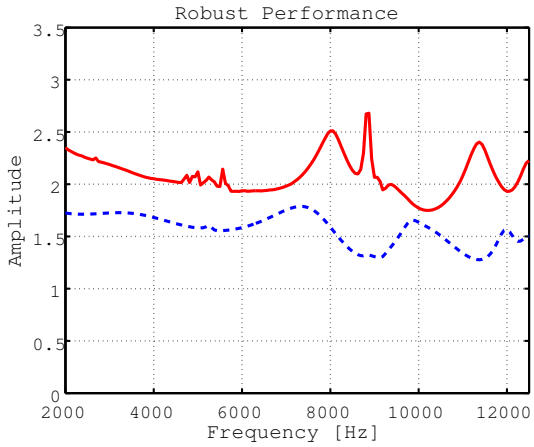

Figure 13: Frequency dependent curves to compute RMS values. The means of the areas below the curves are RMS values ($\log_{10}$-scaled). The dashed line is a corresponding curve for nominal performance.

controller, C_0, of order 6. The corresponding sensitivity function is

$$S_0(z) := \frac{1}{1 + G(z)C_0(z)}, \tag{9}$$

This controller gives the nominal performance (i.e., the RMS value of y_{pes}) as 5.1589. Robust stability against parametric uncertainties in G_v in (1) and G_m in (2), same

as in Table 3, has been verified by means of μ analysis [9]; see the μ plot in Figure 16.

Since robust stability is sufficiently satisfied by the lead-lag controller C_0, we may be able to improve the nominal performance without losing robust stability. To this end, we shall modify slightly the frequency response of S_0 using the sensitivity shaping technique. The main idea in the design is to push forward the bandwidth, with a care of not losing robust stability. By the design, we have obtained a controller of order 16. The Bode plots of a designed sensitivity function S and the original sensitivity function S_0 are shown in Figure 17. Nominal performance is 4.5884, about 11% better than the original design.

Now, for the obtained controller, we will study robust stability and robust performance, assuming parametric uncertainties in G_v and G_m as in Table 3. For robust stability, the μ plot is drawn in Figure 18, from which it can be verified that the new design still maintains robust stability.

Next, we compute robust performance, which is the upper bound of RMS value of y_{pes} for the worst uncertainty combination. We use the result in [10] for the computation, the result of which is provided in Figure 19. Robust performance is the square root of the mean of the area below the curve in Figure 19, and is calculated as 10.3803. Slightly larger robust performance than that of the initial design and

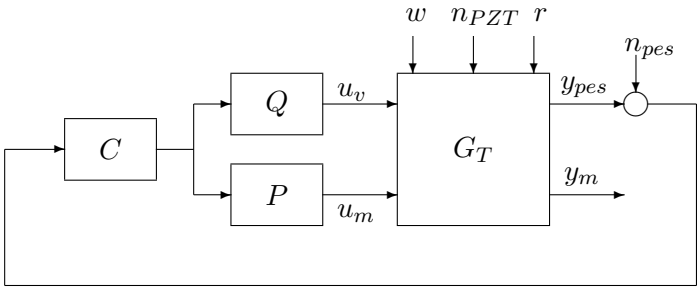

Figure 14: A structure for the PQ design.

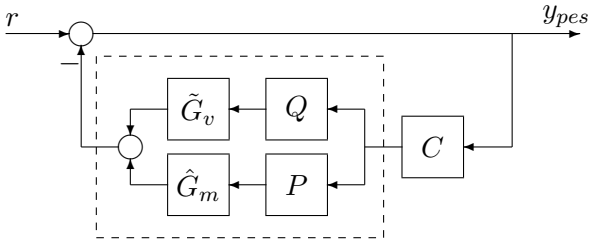

Figure 15: The transfer function from r to y_{pes}.

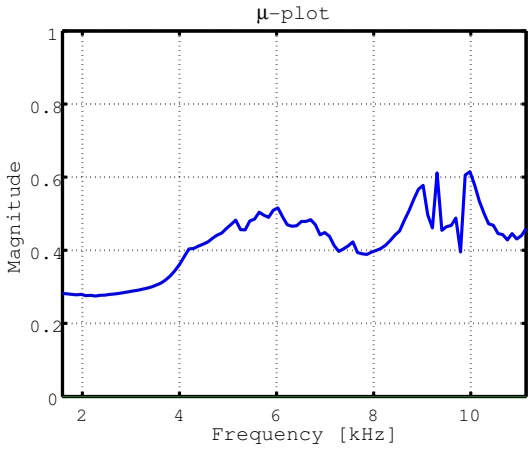

Figure 16: μ plot for parametric uncertainties (initial design).

higher order of the controller are the prices that we pay for achieving smaller nominal performance; see Table 5, where performances of the feedback system with each controller are summarized.

	NP	RP	BW (Hz)	LFG (dB)	$\deg C$
initial design	5.1589	10.2859	14655	-81.2	6
final design	4.5884	10.3803	15649	-80.5	16

Table 5: Summary of performances.

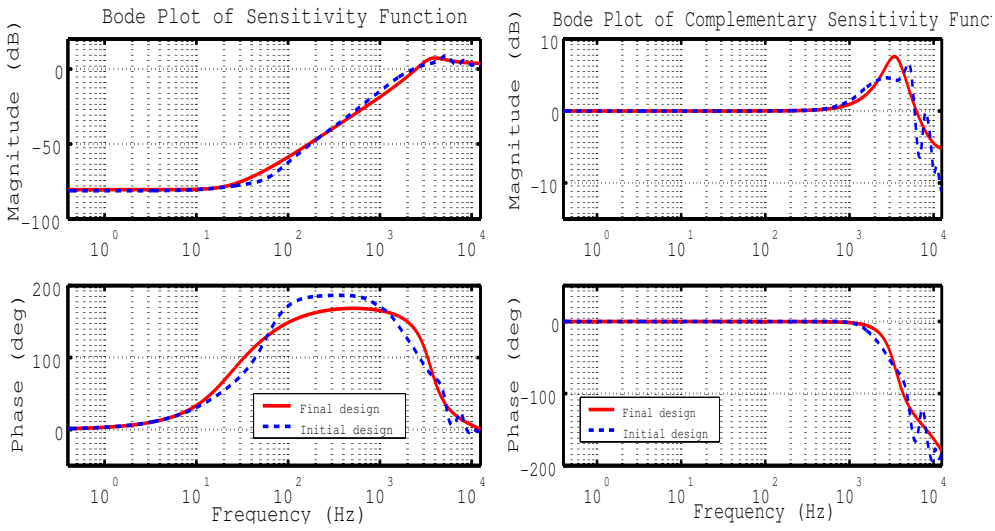

Figure 17: Bode plots of S (left figures) and T (right figures) for the final design (solid) and the initial design (dashed).

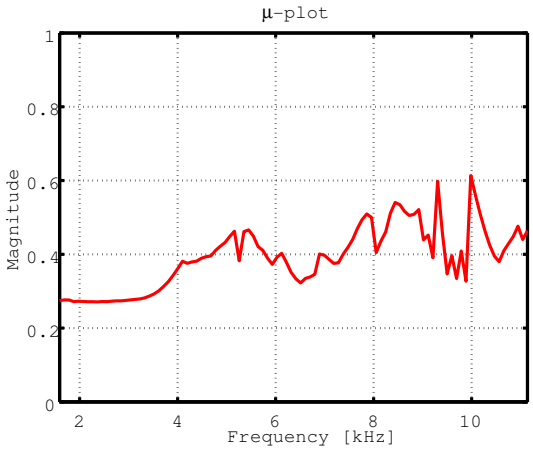

Figure 18: μ plot for parametric uncertainties.

5 Conclusions and discussions

In this paper, we have designed track-following controllers for dual-stage servo systems, using a recently developed technique for sensitivity shaping. Two types of control structures have been considered; one is for the sensitivity decoupling method

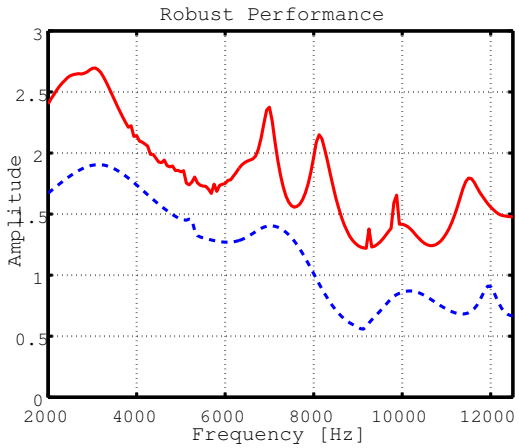

Figure 19: Frequency dependent curves to compute RMS values. The means of the areas below the curves are RMS values ($\log_{10}$-scaled). The dashed line is a corresponding curve for nominal performance.

and the other is for the PQ method. In both cases, we have demonstrated that, by modifying the sensitivity frequency response with the new shaping technique, we can improve nominal performance at a moderate cost of robust stability and performance.

Currently, an overestimating runout model W_r is being used, leading to a conservative result. If we have a more exact/tight runout model, we can take more advantage of the sensitivity shaping technique, especially to obtain a controller of low degree. This can be done by the following procedure. First, we make an LQG controller for the complete model. The LQG controller would be of high order because of the high complexity of the model. This controller gives the best achievable nominal performance. Next, we use the sensitivity function as a reference sensitivity function, and apply our sensitivity shaping technique, with a reduced-order plant. Then, we can bound the degree of controllers, and still try to match the LQG sensitivity, and consequently, to maintain good nominal performance.

In addition, the formulated track-following problem is originally a multivariable

control problem. It would be an interesting topic to apply a multivariable sensitivity shaping technique, which is under investigation, to this control problem directly.

Acknowledgment

This research was supported by grants from Computer Mechanics Laboratory at UC Berkeley (CML) and the Swedish Research Council (VR).

References

[1] D. Abramovitch and G. Franklin. A brief history of disk drive control. *IEEE Control Systems Magazine*, pages 28–42, June 2002.

[2] X. Hu, W. Guo, T. Huang, and B. M. Chen. Discrete-time LQG/LTR dual-stage controller design and implementation for high track density hdds. In *Proc. Amer. Control Conf.*, pages 4111–4115, 1999.

[3] X. Huang, R. Nagamune, R. Horowitz, and Y. Li. Design and analysis of a dual-stage disk drive servo system using an instrumented suspension. In *Proc. of Amer. Control Conf.*, volume 4, pages 535–540, 2004.

[4] Y. Huang, M. Banther, P. D. Mathur, and W. Messner. Design and analysis of a high bandwidth disk drive servo system using an instrumeted suspension. *IEEE/ASME Trans. Mechatronics*, 4(2):196–206, 1999.

[5] Y. Li and R. Horowitz. Mechatronics of electrostatic microactuators for computer disk drive dual-stage servo systems. *IEEE/ASME Trans. Mechatronics*, 6(2):111–121, 2001.

[6] Y. Li and R. Horowitz. Design and testing of track-following controllers for dual-stage servo systems with PZT actuated suspensions. *Microsystem Technologies*, 8:194–205, 2002.

[7] R. Nagamune and A. Blomqvist. Sensitivity shaping with degree constraint by nonlinear least-squares optimization. Technical Report TRITA-MAT-OS02, Royal Institute of Technology, 2004. Available at `http://www.math.kth.se/~andersb`.

[8] K. Oldham, S. Kon, and R. Horowitz. Fabricatin and optimal strain sensor placement in an instrumented disk drive suspension for vibration suppression. Technical Report 10, CML Blue Report, Mechanical Engineering Dept., U. C. Berkeley, Oct. 2003.

[9] A. Packard and J. C. Doyle. The complex structured singular value. *Automatica*, 29(1):71–109, 1993.

[10] F. Paganini. Frequency domain conditions for robust H_2 performance. *IEEE Trans. Automat. Control*, 44(1):38–49, January 1999.

[11] S. J. Schroeck and W. C. Messner. On controller design for linear time-invariant dual-input single-output systems. In *Proc. Amer. Control Conf.*, pages 4122–4126, 1999.

[12] S. J. Schroeck, W. C. Messner, and R. J. McNab. On compensator design for linear time-invariant dual-input single-output systems. *IEEE/ASME Trans. on Mechatronics*, 6(1):50–57, March 2001.

[13] T. Semba, T. Hirano, and L.-S. Fan. Dual-stage servo controller for HDD using MEMS actuator. *IEEE Trans. Magnetics*, 35:2271–2273, Sept 1999.

[14] M. T. White, P. Hingwe, and T. Hirano. Comparison of a MEMS microactuator and a PZT milliactuator for high-bandwidth HDD servo. In *Proc. of Amer. Control Conf.*, volume 3, pages 541–546, 2004.

[15] M. T. White, T. Hirano, H. Yang, K. Scott, S Pattanaik, and F. Y. Huang. High-bandwidth hard disk drive traking using a moving-slider MEMS microactuator. In *Proc. of Advanced Motion Control*, pages 299–304, 2004.

[16] M. T. White and W. M. Lu. Hard disk drive bandwidth limitations due to sampling frequency and computational delay. In *Proc. Int. Conf. Advanced Intelligent Mechatronics*, pages 120–125, 1999.